energies

MDPI

Article

Studies of $FeSe_2$ Cathode Materials for Mg–Li Hybrid Batteries

Changhuan Zhang [1], Liran Zhang [1], Nianwu Li [2] and Xiuqin Zhang [1,*]

[1] Beijing Key Laboratory of Clothing Materials R & D and Assessment, Beijing Engineering Research Center of Textile Nanofiber, Beijing Institute of Fashion Technology, Beijing 100029, China; 20180020@bift.edu.cn (C.Z.); 20180022@bift.edu.cn (L.Z.)

[2] State Key Laboratory of Organic-Inorganic Composites, Beijing University of Chemical Technology, Beijing 100029, China; linianwu@mail.buct.edu.cn

* Correspondence: clyzxq@bift.edu.cn

Received: 8 July 2020; Accepted: 24 August 2020; Published: 25 August 2020



Abstract: Rechargeable magnesium (Mg)-based energy storage has attracted extensive attention in electrochemical storage systems with high theoretical energy densities. The Mg metal is earth-abundant and dendrite-free for the anode. However, there is a strong Coulombic interaction between Mg^{2+} and host materials that often inhibits solid-state diffusion, resulting in a large polarization and poor electrochemical performances. Herein, we develop a Mg–Li hybrid battery using a Mg-metal anode, an $FeSe_2$ powder with uniform size and a morphology utilizing a simple solution-phase method as the counter electrode and all-phenyl-complex/tetrahydrofuran (APC)-LiCl dual-ion electrolyte. In the Li^+-containing electrolyte, at a current density of 15 mA g^{-1}, the Mg–Li hybrid battery (MLIB) delivered a satisfying initial discharge capacity of 525 mAh g^{-1}. Moreover, the capacity was absent in the $FeSe_2$|APC|Mg cell. The working mechanism proposed is the "Li+-only intercalation" at the $FeSe_2$ and the "Mg^{2+} dissolved or deposited" at the Mg foil in the $FeSe_2$|Mg^{2+}/Li^+|Mg cell. Furthermore, ex situ XRD was used to investigate the structural evolution in different charging and discharging states.

Keywords: Mg–Li hybrid batteries; magnesium batteries; $FeSe_2$; metal anode

1. Introduction

The application of magnesium (Mg)-based energy storage technologies in high energy density electrochemical storage systems has attracted increasing attention. The reason why magnesium-based batteries has attracted extensive attention, recently—especially in Mg-metal anode ("negative") batteries—is that Mg is cheap, readily available and has a reasonable reduction potential (−2.4 V vs. SHE) and large specific volumetric capacity of 3833 mAh cm^{-3} (a two-electron transfer process) [1–3]. Additionally, most importantly, rapid deposition and/or exfoliation of Mg is possible in compatible electrolytes without forming dendritic structures [2,4]. However, there is an obstacle to the application of Mg-based energy storage due to its bivalent cation, namely, a strong Coulombic interaction between Mg^{2+} ions (which have higher charge densities than monovalent) and the host materials. This often results in slowing the solid-state diffusion—which then leads to significant polarization and poor electrochemical performance [5,6]. In order to overcome these problems, one approach is to develop better bivalent Mg-ion host cathode materials. Another is to utilize a suitable electrolyte system with Mg-metal anode.

To date, many studies have focused on the cathode materials. The representative cathode materials for rechargeable Mg batteries has been intercalation materials, including Chevrel-phase materials (Mo_6X_8; X = S, Se) [7–9], layered MX materials (where M is a metal; X = S, Se;, i.e., TiS_2, FeS_2, $TiSe_2$,

WSe_2, $CoSe_2$) [10–14], spinel compounds (spinel λ-Mn_2O_4 and sulfur spinel compounds (Mn_2S_4, Cr_2S_4, Ti_2S_4)) [15–17], layered oxide materials (V_2O_5, α-MoO_3, TiO_2, etc.) [18–22] and polyanion materials (transition metal silicates and phosphates) [23–27]. Instead of intercalation materials, the conversion materials have also been important research objects. For example, transition metal oxides (α-MnO_2, δ-MnO_2) [28–31], chalcogenide (CuS, $Cu_2{-}\chi Se$) [32–35], chloride (AgCl) [36] and organic compounds (quinone-based polymers and 2,5-dimethoxy-1,4-benzoquinone (DMBQ)) [37,38]. In addition, it has been found that trace water in the electrolyte could be beneficial for interfacial ion transfer and the ionic diffusion under study. This was named as water co-intercalation materials (α-V_2O_5, δ-MnO_2) [16,30,31]. However, among these materials, only a few exhibit available performance of the Mg-ion battery (MIB). The main reason is the sluggish transportation of Mg ions in the host material.

In order to overcome the obstacle of Mg-ion sluggish solid–state diffusion, the elemental redox chemistries (Mg/O_2, Mg/S, Mg/I_2, Mg/Se) [39–45] and Mg^{2+}/Li^+ (Mg–Li) ion, Mg^{2+}/Na^+ (Mg–Na) ion, Mg^{2+}/Zn^{2+} (Mg–Zn) of ion dual-salt electrolyte systems [26,46–56] has been investigated. Mg–Li hybrid batteries (MLIBs) with $NaV_3O_8{\cdot}1.69H_2O$ (NVO) nanobelts as the cathode and Mg metal as the anode exhibit a high rate capability. The reaction mechanism is the Li^+ intercalated—along with a small amount of Mg^{2+} adsorption at the cathode during the discharging process—whereas the anode side is dominated by Mg^{2+} deposition/dissolution [53]. The sulfur compounds and oxide materials (MoS_2, TiS_2, TiO_2, etc.) have also functioned well in hybrid cells with Li^+-containing APC electrolytes [47–49]. In this regard, the Mg–Li hybrid ion battery is an ideal choice.

During the development of cathode materials—in order to decrease anion polarizability—selenides were investigated as cathodes due to their demonstrated or projected good ionic mobility. Nickel–iron (Ni–Fe) bimetallic diselenides microflowers ($Ni_{0.75}Fe_{0.25}Se_2$, NFS) had been reported [57] as cathodes for rechargeable Mg batteries. The NFS delivered a considerable specific capacity of 190 mAh g^{-1} at 10 mAh g^{-1} in APC electrolyte. Hence, iron diselenide ($FeSe_2$) is a promising candidate material for rechargeable Mg batteries or MLIBs because of its suitable band-gap energy (Eg = 1.0 eV) and good conductivity. The Mg–Li dual salt electrolytes could be used to obtain rapid ion transport within the cathode while maintaining the utility and benefits of an Mg anode.

Herein, $FeSe_2$ powder with uniform size and morphology using a simple solution-phase method was fabricated according the previous report [58] and used as the cathode materials for the MLIBs. Besides the physical investigation for the $FeSe_2$, an electrochemical characterization is carried out for the MLIBs system. The MLIBs system had improved the performance over the rechargeable Mg batteries with the $FeSe_2$ cathode. MLIBs with $FeSe_2$ cathode demonstrating a high initial discharge specific capacity (525 mAh g^{-1} at 15 mA g^{-1}) and relatively good rate capabilities. Moreover, no obvious capacity or voltage plateau was observed for $FeSe_2$ in the APC electrolyte system. In this hybrid cell system, Li^+ intercalation occurs reversibly at the cathode material due to its superior mobility compared to divalent magnesium. Mg strips and plates first appeared at the anode as a result of a higher redox potential (−2.37 V) than Li^+/Li^0 (−3.04 V).

2. Experimental Section

2.1. Synthesis of $FeSe_2$

All reagents were obtained from Sigma-Aldrich as analytical grade and ready-to-use without further refinement. In a 100-mL three-necked flask, 30 mL of oleylamine (OM) and 20 mL of 1-octadecene (ODE) were added at room temperature and heated under nitrogen at 120 °C for 30 min. Then, 2 mmol of $FeCl_2{\cdot}4H_2O$ powder was added to the solution. After stirring vigorously for 30 min, a solution of selenium powder (4 mmol) or OM (8 mL) was added to the flask and stirred for 10 min. The solution temperature rose to 150 °C and was maintained for 30 min before cooling to room temperature. After reaction, excessive ethanol was added to the solution to precipitate the $FeSe_2$ nanoparticles. The precipitate was washed repeatedly with hexane and ethanol, and the product was collected by

centrifugation. Then the material was obtained after drying in a vacuum oven. This was prepared according to a previous report [58].

2.2. Preparation of Electrolyte

The all-phenyl-complex/tetrahydrofuran solution (APC, 0.4 M) was prepared according to a previous report about two-step procedure in the argon-filled glove box [59]. Initially, 0.267 g of aluminum trichloride ($AlCl_3$, anhydrous, 99.99%) was slowly added to 3 mL of tetrahydrofuran (THF, anhydrous, ≥99.9%) with vigorous stirring to form an $AlCl_3$–THF solution. Then, 2 mL of phenyl magnesium chloride (2-M solution in THF) was added dropwise to the $AlCl_3$–THF solution. This solution was vigorously stirred for at least 24 h before being used. Due to the exothermic nature of the above prepared solutions, it is worth noting that their preparation should include cooling. The dual salt (Mg^{2+}/Li^{+}) electrolyte was prepared by adding an appropriate amount of LiCl (0.4 M) to the 0.4-M APC electrolyte. The mixture was stirred for at least 12 h prior to use. The electrolyte is sensitive to moisture and oxidation, so all processes should be performed in a glove box (H_2O/O_2 levels < 0.1 ppm) under argon gas protection.

2.3. Material Characterization

The crystalline structures of samples were identified by X-ray powder diffraction (XRD) using a Rigaku D/max-2500 (Cu Kα radiation, λ = 0.15405 nm, 40 kV/200 mA), within diffraction angles 2θ from 20° to 70° at step size of 0.02°. The sample microstructures were characterized using a JEOL 6701 F field-emission scanning electron microscope (FE-SEM).

2.4. Cells Assembling and Electrochemical Measurements

The slurry was comprised of $FeSe_2$ and super P (SP; 80 wt% and 10 wt%, respectively) with 10 wt% poly (vinyl difluoride) (PVDF) in an N-methyl-2-pyrrolidone (NMP) solution. The doctor blade was employed to coat the slurry onto copper foil (99.6%, Goodfellow). After drying at 80 °C for 12 h, it was punched into disk electrodes with a diameter of 1 cm. The active material loading was about 1 mg cm^{-2}. Study of the electrochemical performance of the $FeSe_2$ involved the use of CR2032 coin-shaped cells with the working $FeSe_2$ electrode, an Mg foil as the counter electrode, Whatman borosilicate glass fiber paper as the separator and 180 µL of 0.4-M APC with and without Li^+ as the electrolyte.

Cycling performances and rate capabilities were measured by an Arbin BT2000 system from 0.3 V to 1.6 V versus Mg^{2+}/Mg. The current density was calculated using the mass percent of $FeSe_2$ nanoparticles in the electrodes. Cyclic voltammograms (CVs) were obtained using an Autolab electrochemical workstation (PG302 N) at the same potential range (0.3–1.6 V) and scan rate (0.1 mV s^{-1}, vs. Mg^{2+}/Mg). All electrochemical measurements were carried out at 25 °C.

2.5. Preparation of Ex Situ XRD Samples

To prepare the Mg-containing samples, the pure $FeSe_2$ electrode was discharged to 0.3 V vs. Mg at a constant current of 50 mA g^{-1} while the demagnesiated sample electrodes were charged to 1.6 V vs. Mg. In order to obtain ex situ XRD samples, all cells were disassembled in an inert atmosphere. Moreover, all electrodes were repeatedly washed with THF, then dried overnight at 25 °C to remove excess electrolyte adhering to the surface in an inert atmosphere.

3. Results and Discussion

$FeSe_2$ nanoparticles were synthesized under nitrogen using a simple solution-phase method based on a previous report about synthetic procedure and featured uniform sizes and morphologies [58]. The synthesis procedure of $FeSe_2$ is shown in Figure 1. $FeCl_2{\cdot}4H_2O$ powder and selenium dissolved in OM were sequentially added to a mixed solution of OM and ODE. During the reaction, the $FeCl_2{\cdot}4H_2O$ precursor solution gradually became reddish-yellow. After selenium injection and increasing the

temperature to 150 °C, the color of the solution gradually turned black. The reddish yellow solution was the reaction between $FeCl_2$ and OM which can led to formation of a Fe–OM complex while the black solution was formed of putting Se–OM solution into above solution in order to the formation of $FeSe_2$.

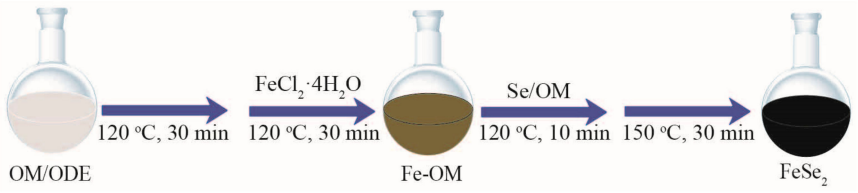


Figure 1. Synthetic route to $FeSe_2$.

The XRD pattern of the as-prepared $FeSe_2$ is shown in Figure 2a, suggesting an orthorhombic $FeSe_2$ structure. The diffraction peaks of the obtained sample matched well with PDF#79-1892 card of $FeSe_2$ Pnnm space group with a lattice parameter a = 4.804 Å, b = 5.784 Å and c = 3.586 Å. The 2θ value of diffraction peak was 31.10, 34.83, 36.23, 48.20, 50.89, 53.95 and 64.05°, respectively. No peaks of any other phases were observed, and the sharp peaks imply the high crystalline structure. It indicated that only high-purity $FeSe_2$ was found in the black solution. The probable reaction mechanism for the formation of $FeSe_2$ was to form a Fe–OM complex through adding the $FeCl_2{\cdot}4H_2O$ powder into the OM/ODE solution. $FeSe_2$ nuclei quickly formed upon the addition of the Se–OM solution and gradually grew over time, ultimately reaching a certain size. The sizes of $FeSe_2$ nanoparticles were well controlled due to the use of OM ligands to protect the surfaces of the material. A scanning electron microscopy (SEM) image of $FeSe_2$ powder are shown in Figure 2b. The SEM confirmed that the $FeSe_2$ had a nanosized dimension, which would be beneficial for enhancing the Mg and Li-ion insertion/extraction during the electrochemical reaction. The nanoparticle of $FeSe_2$ was about 100–300 nm. However, the SEM shows that the $FeSe_2$ nanoparticles were aggregated, and the size of the agglomerate reaches the micron level. This phenomenon had a negative impact on the Mg-ion insertion/extraction because of the serious size-dependence of magnesium storage.

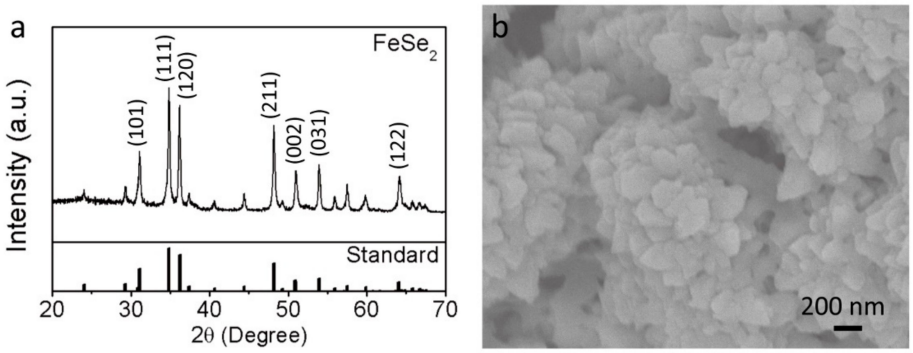


Figure 2. Characterization of $FeSe_2$ nanoparticles. (**a**) XRD spectrum; (**b**) SEM image of $FeSe_2$.

Figure 3a,b shows the CV curves of the $FeSe_2$ electrodes recorded using APC electrolyte with and without LiCl, respectively. It can be observed that the curves of the first cycle was different from the subsequent cycles. For the initial Li^+-containing electrolyte cycle (scanned from an open circuit potential of ~1.65 V, all subsequent potentials now referring to Mg/Mg^{2+}), a cathodic broad peak clearly appeared at 0.58 V can be attributed to the solid electrolyte interphase (SEI) layers formation resulting from the electrochemically driven electrolyte degradation and the decomposition of $FeSe_2$ ($FeSe_2 + 2Li^+ + 2e^- \rightarrow FeSe + Li_2Se$, $FeSe + 2Li^+ + 2e^- \rightarrow Fe + Li_2Se$) (Figure 4a) [60,61]. Two anodic peaks appeared at approximately 1.21 and 1.56 V in the subsequent CV scans in the first cycle, respectively, which should be ascribed to the formation of the Li_xFeSe and FeSe ($Fe + Li_2Se \rightarrow$

$Li_xFeSe + (2-x)Li^+ + (2-x)e^-$, $Li_xFeSe \rightarrow FeSe + xLi^+ + xe^-$), respectively (Figure 4a) [60,61]. During the subsequent cycles, both peak intensity and positions changed. There were two cathodic peaks at ~0.61 and 1.06 V, which could be corresponded to the decomposition of $FeSe_2$ and FeSe. While two anodic peaks appeared at ~1.16 and 1.48 V, it could be ascribed to the formation of the Li_xFeSe and FeSe. It exhibited a relatively high symmetry with cathodic peak and anodic peak, but the current density of cathode/anode peak gradually decreased with increasing cycles. This is likely that due to the reversible phase transition induced by Li^+ intercalation and deintercalation in the Li^+-containing electrolyte. In contrast, in the APC electrolyte without addition of LiCl, cathodic and anodic peaks appeared in the first cycles. The subsequent cycles showed negligible currents, indicating that the Mg^{2+} was almost irreversible for the $FeSe_2$ electrode. These peaks were corresponded to small plateaus presented in the charge–discharge curves (Figure 3c,d).

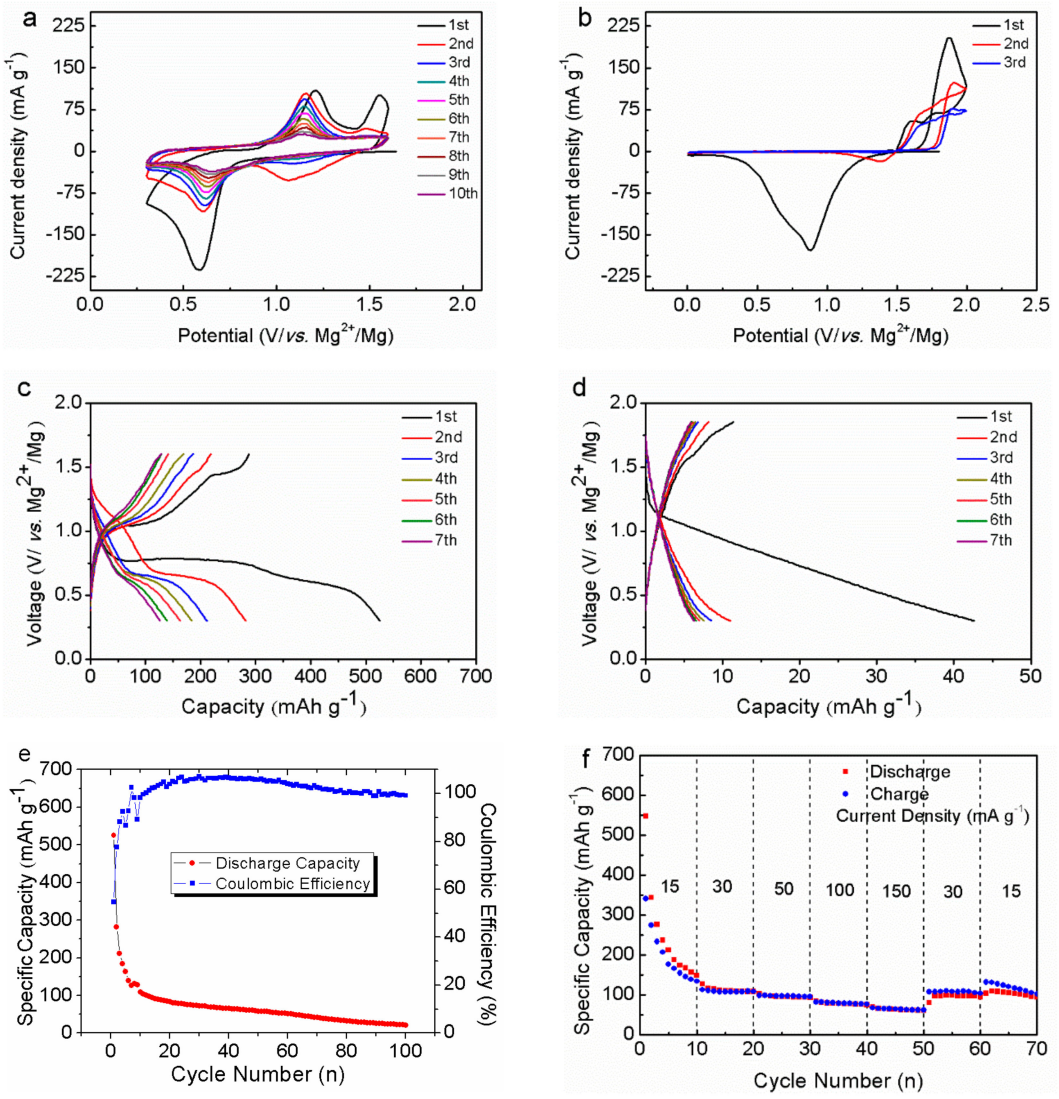


Figure 3. CV curves of (**a**) $FeSe_2|Mg^{2+}/Li^+|Mg$ cell and (**b**) $FeSe_2|Mg^{2+}|Mg$ cell; charge–discharge curves of (**c**) $FeSe_2|Mg^{2+}/Li^+|Mg$ cell and (**d**) $FeSe_2|Mg^{2+}|Mg$ cell; (**e**) cycling performance and Coulombic efficiency of $FeSe_2|Mg^{2+}/Li^+|Mg$ cell; (**f**) rate capability of $FeSe_2|Mg^{2+}/Li^+|Mg$ cell.

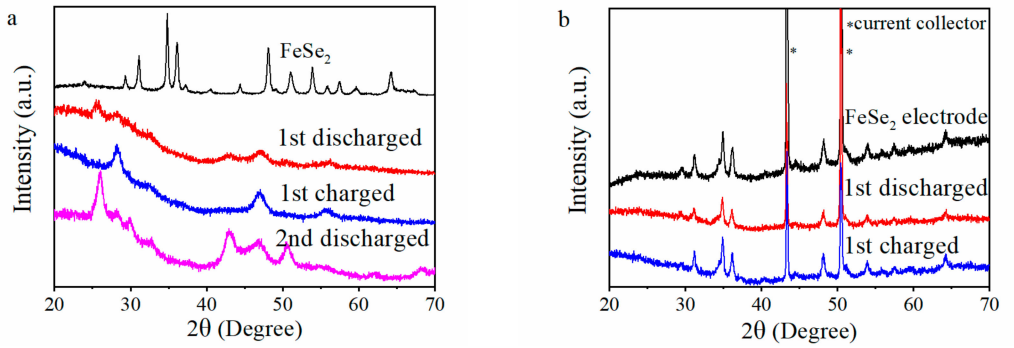


Figure 4. XRD patterns of the $FeSe_2$ electrode in (**a**) $FeSe_2|Mg^{2+}/Li^+|Mg$ cell and (**b**) $FeSe_2|Mg^{2+}|Mg$ cell at different discharging/charging states.

Figure 3c,d showed the charge–discharge curves of the $FeSe_2$ electrode cycled at constant specific current (15 mA g^{-1}) using APC electrolyte with and without LiCl, respectively. In the Li^+-containing APC electrolyte, the $FeSe_2|Mg^{2+}/Li^+|Mg$ cell delivered initial specific capacities of 525 and 287 mAh g^{-1} with a low Coulombic efficiency of 55%, respectively, although the capacities decreased with the increase of cycle number. This capacity value was significantly higher than the $FeSe_2|Mg^{2+}|Mg$ cell. For the APC electrolyte without LiCl, the $FeSe_2|Mg^{2+}|Mg$ cell delivered initial discharge and charge capacities of 42 and 11 mAh g^{-1}, respectively. Moreover, it delivered very little capacity during subsequent cycles. These results were consistent with the CV curves and had shown that the reaction mechanism of this material in the Mg–Li hybrid (or dual salt) cell may be attributed to lithiation/delithiation rather than magnesiation/demagnesiation.

The cycling performances and Coulombic efficiency of $FeSe_2|Mg^{2+}/Li^+|Mg$ battery are illustrated in Figure 3e. As is seen from the curves, the specific capacities decreased with the increase of cycles. In addition—despite a lower Coulombic efficiency observed in the first and second cycles—the Mg–Li hybrid battery showed a highly reversible behavior during subsequent cycles. The chloride ion was the counter-ion for the lithium salt, which made up a part of APC, and LiCl was expected to be very compatible with APC. The formed APC–LiCl electrolyte was conducive to highly reversible Mg deposition and/or dissolution and afforded a high anodic stability, despite the reaction between LiCl and the complex Mg electrolyte [62]. Low initial Coulombic efficiencies at first may be due to the SEI formation. For comparison, the rate capabilities of the $FeSe_2|Mg^{2+}/Li^+|Mg$ battery under various current densities are shown in Figure 3f. Raising the current density from 15 mA g^{-1} to 150 mA g^{-1}, the capacity decreased the increase of current density. This reflected a relatively favorable capability during short cycling. The results showed that the performance of the MLIBs was superior to the traditional rechargeable Mg battery.

The electrochemical reaction mechanism of the $FeSe_2$ was further investigated by ex situ X-ray diffraction (XRD) test at different discharging/charging states in APC electrolytes with and without LiCl. The results are shown in Figure 4a,b, respectively. In the Li^+-containing electrolyte, the "Li+-only intercalation" mechanism at the cathode was confirmed after a comparison of XRD patterns before and after discharging (Figure 4a). After discharging at first time, the Li_2Se, Fe and FeSe were detected, it can be attributed to the solid electrolyte interphase (SEI) layers formation resulting from the electrochemically driven electrolyte degradation and the decomposition of $FeSe_2$ ($FeSe_2 + 2Li^+ + 2e^- \rightarrow FeSe + Li_2Se$, $FeSe + 2Li^+ + 2e^- \rightarrow Fe + Li_2Se$) [60,61]. This confirmed that only Li^+ reacted with $FeSe_2$ in the mixed-ion electrolyte and was consistent with the CV and charge–discharge curves. However, after charging at first time, the FeSe was detected rather than $FeSe_2$. Which should be ascribed to the formation of the Li_xFeSe and FeSe ($Fe + Li_2Se \rightarrow Li_xFeSe + (2\text{-}x)Li^+ + (2\text{-}x)e^-$, $Li_xFeSe \rightarrow FeSe + xLi^+ + xe^-$), respectively [60,61]. In the plain APC electrolyte, the $FeSe_2$ structure remained unchanged during the charge–discharge process (Figure 4b).

Based on the above analyses, a proposed mechanism is shown in Figure 5. Since Li^+ ions are completely supplied though the electrolyte, this hybrid battery requires high Li^+ concentrations of more than 0.4-M in the electrolyte to function at high capacities.

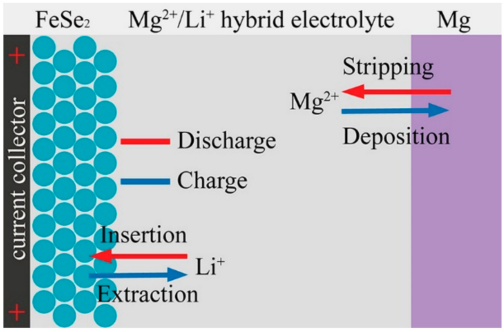


Figure 5. Schematic of the working mechanism of the $FeSe_2|Mg^{2+}/Li^+|Mg$ battery.

4. Conclusions

This study developed a Mg–Li hybrid battery using a Mg-metal anode, an $FeSe_2$ powder with uniform size and morphology utilizing a simple solution-phase method as the counter electrode and an 0.4-M APC electrolyte with 0.4-M LiCl additive. $FeSe_2$ was proved to be a promising cathode material for the Mg^{2+}/Li^+ hybrid electrolyte of rechargeable Mg-anode batteries. In the Li^+-containing electrolyte, at a current density of 15 mA g^{-1}, the MLIB delivered satisfying initial discharge capacity of 525 mAh g^{-1} and charge capacity of 287 mAh g^{-1}, respectively. However, the capacity was absent in the $FeSe_2|Mg^{2+}|Mg$ cell. The proposed working mechanism was the "Li+-only intercalation" at the $FeSe_2$ and the "Mg^{2+} dissolved or deposited" at the Mg foil in the $FeSe_2|Mg^{2+}/Li^+|Mg$ cell. The electrolyte provided all the high concentrations of Li^+ needed, in order that the Mg–Li hybrid battery can function at high capacities.

Author Contributions: C.Z., L.Z. and N.L. carried out the material laboratory work, participated in the design of the study and the manuscript structure; C.Z. collected field data and drafted the manuscript; L.Z., N.L. and X.Z. participated in data analysis and critically revised the manuscript. All authors gave final approval for publication and agree to be held accountable for the work performed therein. All authors have read and agreed to the published version of the manuscript.

Funding: This research was funded by the Key Project Science for Beijing Institute of Fashion Technology, Grant Number 2020A-04; The Special Fund for High-Level Teachers of Beijing Institute of Fashion Technology, Grant Number BIFTXJ201917; The Technological Winter Olympics-Research and Development of High-performance and Multifunctional Winter Olympics Clothing, Grant Number Z181100005918005; The Beijing Great Wall Scholars Incubator Program, Grant Number CTT&TCD20180321; The Science and Technology Innovation Service Capacity Building-Basic Research Fund, Grant Number KJCX1902-30299/001.

Acknowledgments: Authors are grateful to other members of our group for their feedback on earlier versions of the study. The authors thanks anonymous reviewers and editors for helpful suggestions on the manuscript.

Conflicts of Interest: The authors declare no conflict of interest.

References

1. Yoo, H.D.; Shterenberg, I.; Gofer, Y.; Gershinsky, G.; Pour, N.; Aurbach, D. Mg rechargeable batteries: An on-going challenge. *Energy Environ. Sci.* **2013**, *6*, 2265–2279. [CrossRef]
2. Mao, M.; Gao, T.; Hou, S.; Wang, F.; Chen, J.; Wei, Z.; Fan, X.; Ji, X.; Ma, J.; Wang, C. High energy density rechargeable Mg battery enabled by a displacement reaction. *Nano Lett.* **2019**, *19*, 6665–6672. [CrossRef] [PubMed]
3. Kuganathan, N.; Gkanas, E.I.; Chroneos, A. Mg_6MnO_8 as a Magnesium-Ion Battery Material: Defects, Dopants and Mg-Ion Transport. *Energies* **2019**, *12*, 3213. [CrossRef]
4. Aurbach, D.; Cohen, Y.; Moshkovich, M. The study of reversible magnesium deposition by in situ scanning tunneling microscopy. *Electrochem. Solid State Lett.* **2001**, *4*, A113–A116. [CrossRef]

5. Muldoon, J.; Bucur, C.B.; Gregory, T. Quest for nonaqueous multivalent secondary batteries: Magnesium and beyond. *Chem. Rev.* **2014**, *114*, 11683–11720. [CrossRef] [PubMed]
6. Ponrouch, A.; Rosa Palacin, M. Post-Li batteries: Promises and challenges. *Philos. Trans. R. Soc. A Math. Phys. Eng. Sci.* **2019**, *377*, 20180297. [CrossRef]
7. Levi, M.D.; Lancry, E.; Gizbar, H.; Lu, Z.; Levi, E.; Gofer, Y.; Aurbach, D. Kinetic and thermodynamic studies of Mg^{2+} and Li^{+} ion insertion into the Mo_6S_8 Chevrel phase. *J. Electrochem. Soc.* **2004**, *151*, A1044–A1051. [CrossRef]
8. Aurbach, D.; Lu, Z.; Schechter, A.; Gofer, Y.; Gizbar, H.; Turgeman, R.; Cohen, Y.; Moshkovich, M.; Levi, E. Prototype systems for rechargeable magnesium batteries. *Nature* **2000**, *407*, 724–727. [CrossRef]
9. Saha, P.; Jampani, P.H.; Datta, M.K.; Hong, D.; Gattu, B.; Patel, P.; Kadakia, K.S.; Manivannan, A.; Kumta, P.N. A rapid solid-state synthesis of electrochemically active Chevrel phases (Mo_6T_8; T = S, Se) for rechargeable magnesium batteries. *Nano Res.* **2017**, *10*, 4415–4435. [CrossRef]
10. Liu, B.; Luo, T.; Mu, G.; Wang, X.; Chen, D.; Shen, G. Rechargeable Mg-ion batteries based on WSe_2 nanowire cathodes. *ACS Nano* **2013**, *7*, 8051–8058. [CrossRef]
11. Liu, Y.; Jiao, L.; Wu, Q.; Zhao, Y.; Cao, K.; Liu, H.; Wang, Y.; Yuan, H. Synthesis of rGO-supported layered MoS_2 for high-performance rechargeable Mg batteries. *Nanoscale* **2013**, *5*, 9562–9567. [CrossRef] [PubMed]
12. Zhang, Y.; Chen, D.; Li, X.; Shen, J.; Chen, Z.; Cao, S.-a.; Li, T.; Xu, F. a-MoS_3@CNT nanowire cathode for rechargeable Mg batteries: A pseudocapacitive approach for efficient Mg-storage. *Nanoscale* **2019**, *11*, 16043–16051. [CrossRef] [PubMed]
13. Juran, T.R.; Smeu, M. $TiSe_2$ cathode for beyond Li-ion batteries. *J. Power Sources* **2019**, *436*, 226813. [CrossRef]
14. Chen, D.; Zhang, Y.; Li, X.; Shen, J.; Chen, Z.; Cao, S.-a.; Li, T.; Xu, F. $CoSe_2$ hollow microspheres, nano-polyhedra and nanorods as pseudocapacitive Mg-storage materials with fast solid-state Mg^{2+} diffusion kinetics. *Nanoscale* **2019**, *11*, 23173–23181. [CrossRef] [PubMed]
15. Liu, M.; Rong, Z.; Malik, R.; Canepa, P.; Jain, A.; Ceder, G.; Persson, K.A. Spinel compounds as multivalent battery cathodes: A systematic evaluation based on ab initio calculations. *Energ. Environ. Sci.* **2015**, *8*, 964–974. [CrossRef]
16. Kim, C.; Phillips, P.J.; Key, B.; Yi, T.; Nordlund, D.; Yu, Y.-S.; Bayliss, R.D.; Han, S.-D.; He, M.; Zhang, Z.; et al. Direct observation of reversible magnesium ion intercalation into a spinel oxide host. *Adv. Mater.* **2015**, *27*, 3377–3384. [CrossRef]
17. Liu, M.; Jain, A.; Rong, Z.; Qu, X.; Canepa, P.; Malik, R.; Ceder, G.; Persson, K.A. Evaluation of sulfur spinel compounds for multivalent battery cathode applications. *Energ. Environ. Sci.* **2016**, *9*, 3201–3209. [CrossRef]
18. Attias, R.; Salama, M.; Hirsch, B.; Gofer, Y.; Aurbach, D. Solvent effects on the reversible intercalation of magnesium-ions into V_2O_5 electrodes. *Chemelectrochem* **2018**, *5*, 3514–3524. [CrossRef]
19. Mukherjee, A.; Sa, N.; Phillips, P.J.; Burrell, A.; Vaughey, J.; Klie, R.F. Direct investigation of Mg intercalation into the orthorhombic V_2O_5 cathode using atomic-resolution transmission electron microscopy. *Chem. Mater.* **2017**, *29*, 2218–2226. [CrossRef]
20. Barnes, T.A.; Wan, L.F.; Kent, P.R.C.; Prendergast, D. Hybrid DFT investigation of the energetics of Mg ion diffusion in alpha-MoO_3. *Phys. Chem. Chem. Phys.* **2018**, *20*, 24877–24884. [CrossRef]
21. Wang, Y.; Xue, X.; Liu, P.; Wang, C.; Yi, X.; Hu, Y.; Ma, L.; Zhu, G.; Chen, R.; Chen, T.; et al. Atomic substitution enabled synthesis of vacancy-rich two-dimensional black TiO2-x nanoflakes for high-performance rechargeable magnesium batteries. *ACS Nano* **2018**, *12*, 12492–12502. [CrossRef] [PubMed]
22. Koketsu, T.; Ma, J.; Morgan, B.J.; Body, M.; Legein, C.; Dachraoui, W.; Giannini, M.; Demortiere, A.; Salanne, M.; Dardoize, F.; et al. Reversible magnesium and aluminium ions insertion in cation-deficient anatase TiO_2. *Nat. Mater.* **2017**, *16*, 1142–1146. [CrossRef] [PubMed]
23. Li, Y.; Nuli, Y.; Yang, J.; Yilinuer, T.; Wang, J. $MgFeSiO_4$ prepared via a molten salt method as a new cathode material for rechargeable magnesium batteries. *Chin. Sci. Bull.* **2011**, *56*, 386–390. [CrossRef]
24. Feng, Z.; Yang, J.; NuLi, Y.; Wang, J. Sol-gel synthesis of $Mg_{1.03}Mn_{0.97}SiO_4$ and its electrochemical intercalation behavior. *J. Power Sources* **2008**, *184*, 604–609. [CrossRef]
25. Huang, Z.-D.; Masese, T.; Orikasa, Y.; Mori, T.; Minato, T.; Tassel, C.; Kobayashi, Y.; Kageyama, H.; Uchimoto, Y. $MgFePO_4F$ as a feasible cathode material for magnesium batteries. *J. Mater. Chem. A* **2014**, *2*, 11578–11582. [CrossRef]

26. Rubio, S.; Liu, R.; Liu, X.; Lavela, P.; Tirado, J.L.; Li, Q.; Liang, Z.; Ortiz, G.F.; Yang, Y. Exploring the high-voltage Mg^{2+}/Na^{+} co-intercalation reaction of $Na_3VCr(PO_4)_3$ in Mg-ion batteries. *J. Mater. Chem. A* **2019**, *7*, 18081–18091. [CrossRef]
27. Zeng, J.; Yang, Y.; Lai, S.; Huang, J.; Zhang, Y.; Wang, J.; Zhao, J. A promising high-voltage cathode material based on mesoporous $Na_3V_2(PO_4)_3$/C for rechargeable magnesium batteries. *Chem. Eur. J.* **2017**, *23*, 16898–16905. [CrossRef]
28. Zhijun, J.; Jiawei, H.; Lujing, L.; Yi, W.; Tao, Q. Vertically aligned alpha-MnO_2 nanosheets on carbon nanotubes as cathodic materials for aqueous rechargeable magnesium ion battery. *Ionics* **2018**, *24*, 3483–3491. [CrossRef]
29. Zhang, R.; Yu, X.; Nam, K.-W.; Ling, C.; Arthur, T.S.; Song, W.; Knapp, A.M.; Ehrlich, S.N.; Yang, X.-Q.; Matsui, M. alpha-MnO_2 as a cathode material for rechargeable Mg batteries. *Electrochem. Commun.* **2012**, *23*, 110–113. [CrossRef]
30. Sun, X.; Duffort, V.; Mehdi, B.L.; Browning, N.D.; Nazar, L.F. Investigation of the mechanism of Mg insertion in birnessite in nonaqueous and aqueous rechargeable Mg-ion batteries. *Chem. Mater.* **2016**, *28*, 534–542. [CrossRef]
31. Nam, K.W.; Kim, S.; Lee, S.; Salama, M.; Shterenberg, I.; Gofer, Y.; Kim, J.-S.; Yang, E.; Park, C.S.; Kim, J.-S.; et al. The high performance of crystal water containing manganese birnessite cathodes for magnesium batteries. *Nano Lett.* **2015**, *15*, 4071–4079. [CrossRef] [PubMed]
32. Duffort, V.; Sun, X.; Nazar, L.F. Screening for positive electrodes for magnesium batteries: A protocol for studies at elevated temperatures. *Chem. Commun.* **2016**, *52*, 12458–12461. [CrossRef] [PubMed]
33. Xiong, F.; Fan, Y.; Tan, S.; Zhou, L.; Xu, Y.; Pei, C.; An, Q.; Mai, L. Magnesium storage performance and mechanism of CuS cathode. *Nano Energy* **2018**, *47*, 210–216. [CrossRef]
34. Liu, H.; Shi, X.; Xu, F.; Zhang, L.; Zhang, W.; Chen, L.; Li, Q.; Uher, C.; Day, T.; Snyder, G.J. Copper ion liquid-like thermoelectrics. *Nat. Mater.* **2012**, *11*, 422–425. [CrossRef]
35. Chen, D.; Zhang, Y.; Li, X.; Shen, J.; Chen, Z.; Cao, S.-a.; Li, T.; Xu, F. Nanosheets assembling hierarchical starfish-like $Cu_{2-x}Se$ as advanced cathode for rechargeable Mg batteries. *Chem. Eng. J.* **2020**, *384*, 123235. [CrossRef]
36. Zhang, R.; Ling, C.; Mizuno, F. A conceptual magnesium battery with ultrahigh rate capability. *Chem. Commun.* **2015**, *51*, 1487–1490. [CrossRef]
37. Pan, B.; Huang, J.; Feng, Z.; Zeng, L.; He, M.; Zhang, L.; Vaughey, J.T.; Bedzyk, M.J.; Fenter, P.; Zhang, Z.; et al. Polyanthraquinone-based organic cathode for high-performance rechargeable magnesium-ion batteries. *Adv. Energy. Mater.* **2016**, *6*, 1600140. [CrossRef]
38. Pan, B.; Zhou, D.; Huang, J.; Zhang, L.; Burrell, A.K.; Vaughey, J.T.; Zhang, Z.; Liao, C. 2,5-Dimethoxy-1,4-Benzoquinone (DMBQ) as organic cathode for rechargeable magnesium-ion batteries. *J. Electrochem. Soc.* **2016**, *163*, A580–A583. [CrossRef]
39. Vardar, G.; Smith, J.G.; Thomson, T.; Inagaki, K.; Naruse, J.; Hiramatsu, H.; Sleightholme, A.E.S.; Sakamoto, J.; Siegel, D.J.; Monroe, C.W. Mg/O_2 battery based on the magnesium-aluminum chloride complex (MACC) electrolyte. *Chem. Mater.* **2016**, *28*, 7629–7637. [CrossRef]
40. Li, W.; Cheng, S.; Wang, J.; Qiu, Y.; Zheng, Z.; Lin, H.; Nanda, S.; Ma, Q.; Xu, Y.; Ye, F.; et al. Synthesis, crystal structure, and electrochemical properties of a simple magnesium electrolyte for magnesium/sulfur batteries. *Angew. Chem. Int. Ed.* **2016**, *55*, 6406–6410. [CrossRef]
41. Fan, H.; Zheng, Z.; Zhao, L.; Li, W.; Wang, J.; Dai, M.; Zhao, Y.; Xiao, J.; Wang, G.; Ding, X.; et al. Extending cycle life of Mg/S battery by activation of Mg anode/electrolyte interface through an LiCl-assisted $MgCl_2$ solubilization mechanism. *Adv. Funct. Mater.* **2019**, *30*, 1909370. [CrossRef]
42. Xu, Y.; Zhou, G.; Zhao, S.; Li, W.; Shi, F.; Li, J.; Feng, J.; Zhao, Y.; Wu, Y.; Guo, J.; et al. Improving a Mg/S Battery with YCl_3 Additive and Magnesium Polysulfide. *Adv. Sci.* **2019**, *6*, 1800981. [CrossRef]
43. Gao, T.; Ji, X.; Hou, S.; Fan, X.; Li, X.; Yang, C.; Han, F.; Wang, F.; Jiang, J.; Xu, K.; et al. Thermodynamics and kinetics of sulfur cathode during discharge in $MgTFSI_2$-DME electrolyte. *Adv. Mater.* **2018**, *30*, 1704313. [CrossRef]
44. Tian, H.; Gao, T.; Li, X.; Wang, X.; Luo, C.; Fan, X.; Yang, C.; Suo, L.; Ma, Z.; Han, W.; et al. High power rechargeable magnesium/iodine battery chemistry. *Nat. Commun.* **2017**, *8*, 14083. [CrossRef] [PubMed]
45. Wu, D.; Wang, W.; NuLi, Y.; Yang, J.; Wang, J. Effect of copper to Selenium@Microporous carbon cathode for Mg-Se batteries with nucleophilic electrolyte. *Electrochim. Acta* **2020**, *330*, 135354. [CrossRef]

46. Liu, F.; Liu, Y.; Zhao, X.; Liu, K.; Yin, H.; Fan, L.-Z. Prelithiated V2C MXene: A high-performance electrode for hybrid magnesium/lithium-ion batteries by ion cointercalation. *Small* **2020**, *16*, 1906076. [CrossRef]
47. Fan, X.; Gaddam, R.R.; Kumar, N.A.; Zhao, X.S. A hybrid Mg^{2+}/Li^{+} battery based on interlayer-expanded MoS_2/graphene cathode. *Adv. Energy Mater.* **2017**, *7*, 1700317. [CrossRef]
48. Gao, T.; Han, F.; Zhu, Y.; Suo, L.; Luo, C.; Xu, K.; Wang, C. Hybrid Mg^{2+}/Li^{+} battery with long cycle life and high rate capability. *Adv. Energy. Mater.* **2015**, *5*, 1401507. [CrossRef]
49. Su, S.; Huang, Z.; Nuli, Y.; Tuerxun, F.; Yang, J.; Wang, J. A novel rechargeable battery with a magnesium anode, a titanium dioxide cathode, and a magnesium borohydride/tetraglyme electrolyte. *Chem. Commun.* **2015**, *51*, 2641–2644. [CrossRef]
50. Asif, M.; Rashad, M.; Ali, Z.; Ahmed, I. Synthesis of ternary metal oxides as positive electrodes for Mg-Li hybrid ion batteries. *Nanoscale* **2020**, *12*, 924–932. [CrossRef]
51. Huang, H.; Zhao, G.; Zhang, N.; Sun, K. Two-dimensional Nb_2O_5 holey nanosheets prepared by a graphene sacrificial template method for high performance Mg^{2+}/Li^{+} hybrid ion batteries. *Nanoscale* **2019**, *11*, 16222–16227. [CrossRef] [PubMed]
52. Soundharrajan, V.; Sambandam, B.; Kim, S.; Mathew, V.; Jo, J.; Kim, S.; Lee, J.; Islam, S.; Kim, K.; Sun, Y.-K.; et al. Aqueous magnesium zinc hybrid battery: An advanced high-voltage and high-energy $MgMn_2O_4$ cathode. *ACS Energy Lett.* **2018**, *3*, 1998–2004. [CrossRef]
53. Rashad, M.; Li, X.; Zhang, H. Magnesium/Lithium-Ion hybrid battery with high reversibility by employing $NaV_3O_8{\cdot}1.69H_2O$ nanobelts as a positive electrode. *ACS Appl. Mater. Interfaces* **2018**, *10*, 21313–21320. [CrossRef] [PubMed]
54. Chen, X.; Wang, S.; Wang, H. High performance hybrid Mg-Li ion batteries with conversion cathodes for low cost energy storage. *Electrochim. Acta* **2018**, *265*, 175–183. [CrossRef]
55. Kravchyk, K.V.; Walter, M.; Kovalenko, M.V. A high-voltage concept with sodium-ion conducting beta-alumina for magnesium-sodium dual-ion batteries. *Commun. Chem.* **2019**, *2*, 84. [CrossRef]
56. Miao, Q.; Nuli, Y.; Wang, N.; Yang, J.; Wang, J.; Hirano, S.-i. Effect of Mg^{2+}/Li^{+} mixed electrolytes on a rechargeable hybrid battery with Li4Ti5O12 cathode and Mg anode. *RSC Adv.* **2016**, *6*, 3231–3234. [CrossRef]
57. Zhou, L.; Xiong, F.; Tan, S.; An, Q.; Wang, Z.; Yang, W.; Tao, Z.; Yao, Y.; Chen, J.; Mai, L. Nickel-iron bimetallic diselenides with enhanced kinetics for high-capacity and long-life magnesium batteries. *Nano Energy* **2018**, *54*, 360–366. [CrossRef]
58. Fu, T.; Chen, Y.; Hao, J.; Wang, X.; Liu, G.; Li, Y.; Liu, Z.; Cheng, L. Facile preparation of uniform $FeSe_2$ nanoparticles for PA/MR dual-modal imaging and photothermal cancer therapy. *Nanoscale* **2015**, *7*, 20757–20768. [CrossRef]
59. Mizrahi, O.; Amir, N.; Pollak, E.; Chusid, O.; Marks, V.; Gottlieb, H.; Larush, L.; Zinigrad, E.; Aurbach, D. Electrolyte solutions with a wide electrochemical window for recharge magnesium batteries. *J. Electrochem. Soc.* **2008**, *155*, A103–A109. [CrossRef]
60. Wang, H.; Wang, X.; Li, Q.; Li, H.; Xu, J.; Li, X.; Zhao, H.; Tang, Y.; Zhao, G.; Li, H.; et al. Constructing three-dimensional porous carbon framework embedded with $FeSe_2$ nanoparticles as an anode material for rechargeable batteries. *ACS Appl. Mater. Interfaces* **2018**, *10*, 38862–38871. [CrossRef]
61. Zhong, D.; Chen, J.; Zhang, J.; Luo, Y.; Li, Z.; Cheng, L.; Chen, Y.; Wang, G.; Wang, R. The yolk-shell FeSe@C nanobox with novel synthesis and its high performance for the anode of lithium-ion batteries. *Mater. Res. Express* **2019**, *6*, 085058. [CrossRef]
62. Gofer, Y.; Chusid, O.; Gizbar, H.; Viestfrid, Y.; Gottlieb, H.E.; Marks, V.; Aurbach, D. Improved electrolyte solutions for rechargeable magnesium batteries. *Electrochem. Solid State Lett.* **2006**, *9*, A257–A260. [CrossRef]



© 2020 by the authors. Licensee MDPI, Basel, Switzerland. This article is an open access article distributed under the terms and conditions of the Creative Commons Attribution (CC BY) license (http://creativecommons.org/licenses/by/4.0/).